Achieving High Precision Laparoscopic Manipulation Through Adaptive Force Control

Alexandre Krupa * Guillaume Morel † Michel de Mathelin *

* University of Strasbourg I - LSIIT (CNRS UMR 7005), ENSPS, Bd. S.Brant, 67400 Illkirch, France.

† University of Paris 6 - LRP (CNRS), 10-12 av. de l'Europe, 78140 Vélizy, France.

alexandre.krupa|michel.demathelin@ensps.u-strasbg.fr, morel@robot.uvsq.fr

Abstract

In this paper, we present a new solution to laparoscopic manipulation based on force feedback control. This method allows to both explicitely control the forces applied to the patient through the trocar, and to precisely control the position of the surgical instrument. It does not require any geometrical model of the operative environment, nor any fine robot base placement prior to the instrument insertion. Different control strategies, involving different kinds of sensory equipments are proposed. They are experimentally validated on a laboratory apparatus.

1 Introduction

In the past decade, laparoscopic surgery has been the object of an important research activity in the robotics community. In this application, the robot system has to manipulate a surgical instrument introduced inside the patient's abdomen through an incision point, where a trocar is placed. Usually, this trocar is kinematically modelled as a 2 rotational DOF constraint. Thus, the manipulation is formulated as a 4 DOF problem. Two different kinds of robotic systems have been developed and are now available for a clinical use.

The first strategy, used in the Intuitive Surgical da Vinci system, exploits a 4 DOF robotic device, exhibiting a fixed remote center of rotation placed at the trocar "center" [1, 2]. Such a system suffers from several limitations. First, prior to the insertion of the instrument, the robot base has to be finely placed so that the remote center of rotation precisely fits with the trocar center. In the environment of a surgical room, this may involve a fastidious process. Note that this process may have to be run several times in the same surgical operation. Indeed, in a complex surgical procedure, several trocars are placed in the patient abdomen, and the surgeon needs to use different entry points during the operation, which requires the robot base to be moved. Finally, there is no way of limiting the forces applied to the patient: in case of a displacement of the trocar, due to a motion of the patient, the forces applied to the trocar may increase without any control.

The second strategy for laparoscopic manipulation, proposed by Computer Motion Inc. in the Zeus system, consists of using a 6 DOF device, only four of them being actuated [3]. The two free degrees of freedom are placed in the robot wrist, so that the instrument naturally rotates around the trocar when the wrist center is moved at a given location by the three first joints of the robot. This allows to significantly simplify the robot placement process prior to the operation. Indeed, the robot can be placed independently from the trocar locations in the patient abdomen. The robot can also access, from the same base placement, several entry points. Furthermore, a displacement of the trocar due to a possible motion of the patient does not produce any forces on the trocar. However, this system may also suffer from practical limitations, due to the fact that the 2 DOF rotational constraint is only a rough approximation of the kinematics of the trocar-instrument link. For example, the robot sometimes has to manipulate a thin instrument (*e.g.* 5 mm diameter) through a relatively larger trocar (*e.g.* 15 to 20 mm). Indeed, the choice of the trocar diameter is global for the whole operation and corresponds to the largest instrument that has to be used in the corresponding entry point. Thus, backlash may appear between the instrument and the trocar. Combined with the free DOF of the robot, this may lead to uncontrolled motions of the instrument, and a lack of precision for the surgeon that complicates the manipulation.

This problem is crucial in a research that we are developping in cooperation with IRCAD (Institut de Recherche sur le Cancer de l'Appareil Digestif - Prof. Jacques Marescaux) [4, 5]. In this research, visual servoing is used to control the motion of the instrument from the laparoscope image (see Figure 1). With such an automatic control of the surgical gesture, in some configurations, the backlash between the instrument and the trocar may lead to a cyclic oscillation of the controller.

We propose in this paper a different approach to laparoscopic manipulation that overcomes the above mentioned limitations. The manipulator possesses 6 actuated joints, providing 6 operational degrees of freedom for the instrument. In order to cope with the trocar constraint, a force sensor is placed at the end-effector of the robot. A force controller is then used to explicitely control the lateral forces applied to the trocar towards zero. Different

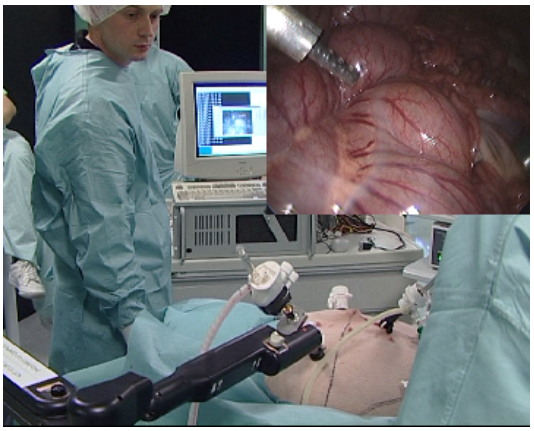

Figure 1: Live experiments of automatic vision based control for laparoscopic surgery using the ComputerMotion's system

control strategies are proposed. Since there is no a priori knowledge of the trocar location with respect to the base, these strategies involve an adaptive estimation of the distance from the end-effector to the trocar center. The paper is organized as follows. Section 2 details the kinematic modelling of laparoscopic manipulation. Section 3 formulates the basic force control loop that is implemented to limit the forces applied to the patient, and shows experimental results. Sections 4 and 5 propose two different strategies to identify on-line the distance from the robot to the trocar. They are both theoretically demonstrated and experimentally validated on a laboratory apparatus.

2 Modelling

We consider a six degrees of freedom robot, equipped with a force sensor, and handling a rigid laparoscopic instrument, that is introduced in a patient's abdomen through a trocar. The kinematics of the laparoscopic manipulation is depicted in Figure 2, where $\mathcal{F}_t = \{O_t, \mathbf{x}_t, \mathbf{y}_t, \mathbf{z}_t\}$ is the tool frame attached to the tip of the instrument, such that the $\mathbf{z}_t$ axis is colinear to the instrument penetration axis ; $\mathcal{F}_s = \{O_s, \mathbf{x}_s, \mathbf{y}_s, \mathbf{z}_s\}$ is the F/T sensor frame, with $\mathbf{z}_s$ colinear to $\mathbf{z}_t$; P is the point of the instrument handler that instantaneously coincides with the trocar ; l is the fixed distance between the origins of $\mathcal{F}_s$ and $\mathcal{F}_t$ and d is the variable distance from P to the origin of $\mathcal{F}_t$. For the sake of simplicity, without loss of generality, it is assumed that the axes of $\mathcal{F}_s$ are aligned with the axes of $\mathcal{F}_t$, that is $\mathbf{x}_t = \mathbf{x}_s$ and $\mathbf{y}_t = \mathbf{y}_s$. The trocar is modelled as a planar kinematic constraint, given by:

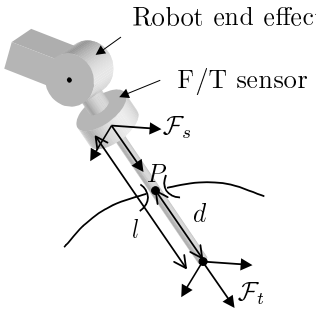

Figure 2: Manipulation through a trocar

$$\mathbf{v}_p^T \mathbf{x}_t = \mathbf{v}_p^T \mathbf{y}_t = 0 \tag{1}$$

where $\mathbf{v}_p$ denotes the velocity of point P, considering the motion of the instrument relatively to the patient. In the sequel, the patient is supposed to be fixed with respect to the robot base. In order to parameter the instantaneous velocity of the instrument with respect to the patient, which is supposed to be fixed, we use the following 4 component operational space vector:

$$\dot{\mathbf{w}} = \begin{pmatrix} \dot{d} & \omega_x & \omega_y & \omega_z \end{pmatrix}^T \tag{2}$$

where $\dot{d} = \mathbf{v}_p^T \mathbf{z}_t$ is the instrument penetration velocity along $\mathbf{z}_t$, and ω_x, ω_y and ω_z are projections of the absolute rotational velocity $\boldsymbol{\omega}$ over $\mathbf{x}_t$, $\mathbf{y}_t$ and $\mathbf{z}_t$ respectively. Combining Equations (1) and (2), one gets:

$$\begin{pmatrix} {}^t\mathbf{v}_p \\ {}^t\boldsymbol{\omega} \end{pmatrix} = \begin{pmatrix} \mathbf{0}_{2\times 4} \\ \mathbf{I}_{4\times 4} \end{pmatrix} \dot{\mathbf{w}} \tag{3}$$

where the upper-left superscript ^{t} indicates that the vector is expressed in the frame $\mathcal{F}_t$, $\mathbf{0}_{2\times 4}$ is a 2-by-4 zero matrix and $\mathbf{I}_{4\times 4}$ is the 4-by-4 identity matrix. Furthermore, the absolute velocity of the instrument at its tip O_t is given by:

$$\begin{pmatrix} {}^t\mathbf{v}_{O_t} \\ {}^t\boldsymbol{\omega} \end{pmatrix} = \mathbf{M}(d) \begin{pmatrix} {}^t\mathbf{v}_p \\ {}^t\boldsymbol{\omega} \end{pmatrix} \tag{4}$$

$$\text{with} \qquad \mathbf{M}(d) = \begin{pmatrix} \mathbf{I}_{3\times 3} & \begin{pmatrix} 0 & d & 0 \\ -d & 0 & 0 \\ 0 & 0 & 0 \end{pmatrix} \\ \mathbf{0}_{3\times 3} & \mathbf{I}_{3\times 3} \end{pmatrix} \tag{5}$$

Conventional robot kinematic modelling can be used to provide the jacobian matrix $\mathbf{J}(q)$ that maps the joint velocity $\dot{q}$ into the instrument tip velocity $\begin{pmatrix} {}^t\mathbf{v}_{O_t}^T & {}^t\boldsymbol{\omega}^T \end{pmatrix}^T$:

$$\begin{pmatrix} {}^t\mathbf{v}_{O_t}^T \\ {}^t\boldsymbol{\omega}^T \end{pmatrix} = \mathbf{J}(q)\dot{q} \tag{6}$$

We finally get the inverse kinematic model:

$$\dot{q} = \mathbf{J}^{-1}(q)\mathbf{M}(d) \begin{pmatrix} \mathbf{0}_{2\times 4} \\ \mathbf{I}_{4\times 4} \end{pmatrix} \dot{\mathbf{w}} \tag{7}$$

where it is assumed that the robot kinematics is non singular. Equation (7) shows that the knowledge of the scalar parameter d is sufficient to provide a robot motion that satisfies the trocar constraint (1). However, in practice, this parameter is not precisely known. Applying equation (7) with an estimated depth $\widehat{d} \neq d$ will provide a lateral motion at the trocar center, thus generating forces. To cope with this problem, force control can be used.

3 Force feedback control

3.1 Control design

Let $\mathbf{f}$ be the force applied by the instrument to the patient through the trocar. We assume here that the interaction force at the instrument tip is negligible. Thus the force $\mathbf{f}$ is directly sensed at the force sensor. The two components of $\mathbf{f}$ along $\mathbf{x}_s = \mathbf{x}_t$ and $\mathbf{y}_s = \mathbf{y}_t$ are $\mathbf{f}_x$ and $\mathbf{f}_y$, respectively. The aim of the force feedback loop is to servo them towards zero. Considering a motion rate control strategy, a simple proportional controller can be used:

$$\begin{cases} \mathbf{x}_t^T \ {}^t\mathbf{v}_p^* = -k\mathbf{f}_x \\ \\ \mathbf{y}_t^T \ {}^t\mathbf{v}_p^* = -k\mathbf{f}_y \end{cases} \tag{8}$$

where ${}^t\mathbf{v}_p^*$ is the control input velocity of point P expressed in $\mathcal{F}_t$. We can now use a hybrid position/force control strategy, that is to control simultaneously the motion $\dot{\mathbf{w}}$ along the four free degrees of freedom and the forces $\mathbf{f}_x$ and $\mathbf{f}_y$ along the two constrained degrees of freedom. This is achieved by the following control law:

$$\begin{aligned} \dot{q}^* &= \mathbf{J}^{-1}(q)\mathbf{M}(\widehat{d}) \left[\begin{pmatrix} \mathbf{0}_{2\times4} \\ \mathbf{I}_{4\times4} \end{pmatrix} \dot{\mathbf{w}}^* - k \begin{pmatrix} \mathbf{I}_{2\times2} \\ \mathbf{0}_{4\times2} \end{pmatrix} \begin{pmatrix} \mathbf{f}_x \\ \mathbf{f}_y \end{pmatrix} \right] \\ &= \mathbf{J}^{-1}(q)\mathbf{M}(\widehat{d}) \begin{pmatrix} -k\mathbf{f}_x \\ -k\mathbf{f}_y \\ \dot{\mathbf{w}}^* \end{pmatrix} \end{aligned} \tag{9}$$

where $\dot{q}^*$ is the joint velocity control input, $\widehat{d}$ is the estimate of d and $\dot{\mathbf{w}}^*$ is the input velocity for the instrument motion. Note that $\dot{\mathbf{w}}^*$ is usually directly set by the surgeon through the teleoperation interface, but it can also be controlled autonomously, from a vision feedback loop, as in [5]. In the sequel, $\mathbf{w}^*$ is supposed to be arbitrary. Also, we will assume, hereafter, that the velocity-controlled robot has a large bandwidth as compared to the external position/force control loop so that:

$$\dot{q} \simeq \dot{q}^* \tag{10}$$

It can be seen in Equation (9) that the distance d has to be estimated in order to implement the control law. Again, this distance is not precisely identified, which can limit the practical efficiency of the force control feedback loop.

3.2 Experimental results

Experiments where performed on a lab apparatus, consisting of a 6 DOF robot, equipped with a force sensor, and manipulating a rigid 0.3 m length surgical instrument through a trocar placed at a surgical endoscopic training device.

For these experiments, the velocity input $\dot{\mathbf{w}}^*$ is set to $(0, \omega_x^*, \omega_y^*, 0)$. The two rotational components are 0.05 Hz, ± 1.5 deg s^{-1} square signals. The objective is to evaluate the influence on the estimation error $\widehat{d} - d$ on the closed loop force control performance. Figure 3 shows the forces $\mathbf{f}_x$ and $\mathbf{f}_y$ measured for different values of $\widehat{d}$ and d. In the first configuration, $\widehat{d} = 0.15$m and $d = 0.2$ m. The maximum forces obtained are $|\mathbf{f}_x| \simeq 2$ N and $|\mathbf{f}_y| \simeq 2$ N. In the second configuration, $\widehat{d} = 0.3$ m and $d = 0.1$ m, the maximum forces are $|\mathbf{f}_x| \simeq 4$ N and $|\mathbf{f}_y| \simeq 5$ N. Finally, in the third configuration, $\widehat{=}0.02$ m and $d = 0.2$, the maximum forces are $|\mathbf{f}_x| \simeq 5$ N and $|\mathbf{f}_y| \simeq 4$ N. Clearly, forces increase with the estimation error on d. is due to the unknown distance d in the control law. These forces are due to the fact that a low gain k has to be used for the force control, so as to guarantee a stable and robust behavior of the force loop. Increasing k would reduce the forces, but may cause chattering in some configurations. Thus,

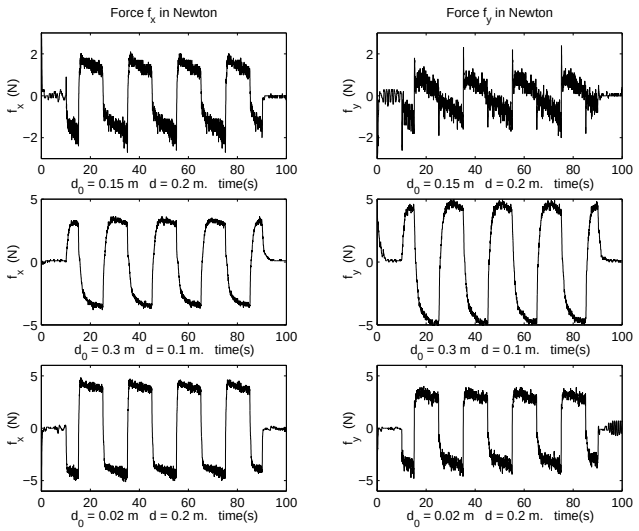

Figure 3: Forces $\mathbf{f}_x$ and $\mathbf{f}_y$ for different values of $\widehat{d}$

it is desirable to provide a way of on-line estimating the penetration depth $\widehat{d}$, in order to obtain a higher performance of the force loop. Two strategies are developed in Sections 4 and 5.

4 Depth estimation with force sensing only

4.1 Adaptive control design

In the first strategy, we consider that the force sensing device only provides a measurement for $\mathbf{f}_x$ and $\mathbf{f}_y$. We then have to reconsider the ideal model given by constraint (1). A residual lateral displacement of point P is introduced:

$$\mathbf{v}_p^T \mathbf{x}_t = \dot{x}_p \qquad \mathbf{v}_p^T \mathbf{y}_t = \dot{y}_p \tag{11}$$

This lateral displacement generates a force. A simplified model of the interaction between the robot and the patient at the incision point is used (like, *e.g.*, in [6, 7]):

$$\mathbf{f}_x = g.x_p \qquad \mathbf{f}_y = g.y_p \tag{12}$$

where g is the stiffness constant of the patient's abdominal wall. Applying the control law (9), and combining

with equations (4), (5), (6), (10), (11) and (12), one gets the following closed loop behavior:

$$\begin{cases} \dot{\mathbf{f}}_x = g\ {}^t\mathbf{v}_p^T\mathbf{x}_t = g\left(-k\mathbf{f}_x + (\widehat{d}-d)\omega_y^*\right) \\ \dot{\mathbf{f}}_y = g\ {}^t\mathbf{v}_p^T\mathbf{y}_t = g\left(-k\mathbf{f}_y - (\widehat{d}-d)\omega_x^*\right) \end{cases} \quad (13)$$

These equations are linear with respect to the parameterization error $(d-\widehat{d})$.
Assuming that g is known, we propose the following normalized gradient algorithm to estimate d:

$$\dot{\widehat{d}} = \dot{d}^* - k_1(\dot{\mathbf{f}}_x + gk\mathbf{f}_x)\frac{\omega_y^*}{\epsilon+\omega_x^{*2}+\omega_y^{*2}} + k_1(\dot{\mathbf{f}}_y + gk\mathbf{f}_y)\frac{\omega_x^*}{\epsilon+\omega_x^{*2}+\omega_y^{*2}} \quad (14)$$

where $k_1 > 0$ is the gain of the gradient algorithm and $\epsilon > 0$ is a normalization coefficient. The stability and convergence properties of this estimation algorithm are given in the following Lemma:

Lemma 1 *:* Stability and convergence properties of the estimation algorithm (14)

1. The estimated parameter $\widehat{d}$ and its derivative are bounded, i.e., $\widehat{d}$, $\dot{\widehat{d}} \in L_\infty$.

2. The error signal $e = \sqrt{\frac{\omega_x^{*2}+\omega_y^{*2}}{\epsilon+\omega_x^{*2}+\omega_y^{*2}}}e_p \in L_2 \cap L_\infty$

3. The parameter estimation error, $e_p = (d-\widehat{d})$, converges, i.e., $\lim_{t\to\infty} e_p = e_{p\infty}$.

4. If $\sqrt{\frac{\omega_x^{*2}+\omega_y^{*2}}{\epsilon+\omega_x^{*2}+\omega_y^{*2}}}$ is persistently exciting, i.e.,

$$\exists\eta>0\ \ \exists T\ \ s.t.\ \ \frac{1}{T}\int_{t_0}^{t_0+T}\frac{\omega_x^{*2}+\omega_y^{*2}}{\epsilon+\omega_x^{*2}+\omega_y^{*2}}dt > \eta > 0 \quad \forall t_0 \geq 0 \quad (15)$$

then, $\lim_{t\to\infty} e_p = 0$, exponentially.

The proof of this Lemma is given in the appendix. We can see that the algorithm is stable and that the convergence of the parameter error to zero is obtained if there is enough excitation (i.e., rotational motions around axis $\mathbf{x}_t$ and $\mathbf{y}_t$). Note that, since a priori $0 < d < l$, a projection is added to always keep the estimate $\widehat{d}$ in the interval $[0, l]$, i.e., $\dot{\widehat{d}} = 0$ if $\widehat{d}$ is 0 or l and its derivative is respectively negative or positive.
In practice, the stiffness parameter may not be known. In this case, noticing that Equation (13) is linear with respect to the stiffness coefficient g, we propose the following gradient algorithm to estimate both parameters g and d on-line:

$$\begin{aligned} \dot{\widehat{d}} &= \dot{d}^* - k_1(\dot{\mathbf{f}}_x + \widehat{g}k\mathbf{f}_x)\omega_y^* + k_1(\dot{\mathbf{f}}_y + \widehat{g}k\mathbf{f}_y)\omega_x^* \\ \dot{\widehat{g}} &= -k_1(\dot{\mathbf{f}}_x + \widehat{g}k\mathbf{f}_x)k\mathbf{f}_x - k_1(\dot{\mathbf{f}}_y + \widehat{g}k\mathbf{f}_y)k\mathbf{f}_y \end{aligned} \quad (16)$$

where $k_1 > 0$ is the gain of this gradient algorithm. The stability and convergence properties of this estimation algorithm are given in the following Lemma:

Lemma 2 *:* Stability and convergence properties of the estimation algorithm (16)

1. $\widehat{d}$, $\widehat{g} \in L_\infty$ and $\dot{\widehat{d}}$, $\dot{\widehat{g}} \in L_\infty$.

2. If $\mathbf{Q}^{\frac{1}{2}}$ is persistently exciting, then $\lim_{t\to\infty} e_p = 0$, exponentially, where $\mathbf{Q} = \mathbf{Q}^T \geq 0$ and

$$\mathbf{Q} = \begin{pmatrix} g^2(\omega_x^{*2}+\omega_y^{*2}) & gk(\mathbf{f}_x\omega_y^* - \mathbf{f}_y\omega_x^*) \\ gk(\mathbf{f}_x\omega_y^* - \mathbf{f}_y\omega_x^*) & k^2\left(\mathbf{f}_x^2+\mathbf{f}_y^2\right) \end{pmatrix}$$

The proof of this Lemma is given in the appendix. We can see that the parameter convergence to zero is obtained if there are rotational motions around $\mathbf{x}_t$ and $\mathbf{y}_t$ as well as translational motions along $\mathbf{x}_t$ and $\mathbf{y}_t$.

4.2 Experimental results

Experiments where conducted on the same lab apparatus, with the same initial conditions. For these experiments, the algorithm (14) has been used, with an a priori knowledge on the interaction stiffness g. This parameter has been roughly identified on the experimental setup. The results are plotted in Figure 4. The convergence of $\hat{d}$ from

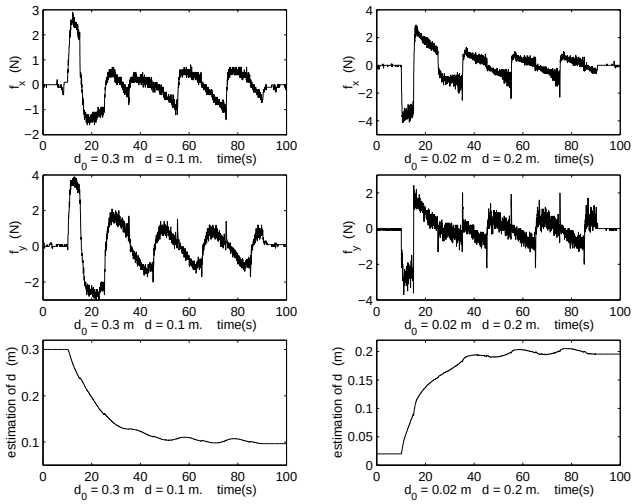

Figure 4: Experimental results - adaptive estimation of d

its initial value d_0 to the real value d is experimentally demonstrated. Together with the convergence of d, one can see that the forces applied to the patient are limited to a reasonable value. Although the measured force suffers fom significant noise, the estimation is smooth. This is due to the low bandwidth of the estimation dynamics that rejects the high frequency noise in $\mathbf{f}$ and $\dot{\mathbf{f}}$, thanks to the use of a low gain k_1. As a price, the convergence is slow. The next section proposes an alternative strategy for a faster identification of d.

5 Robust identification of the distance d from force and torque measurements

5.1 Depth estimation algorithm

In this section, we assume that the whole 6 component interaction wrench can be measured by the force/torque sensor. In this case, the distance, d, can be identified from the measurements of the forces $\mathbf{f}_x$, $\mathbf{f}_y$ and the torques $\boldsymbol{\gamma}_x$, $\boldsymbol{\gamma}_y$. Indeed, we have:

$$m = l - d = \frac{\sqrt{\boldsymbol{\gamma}_x^2 + \boldsymbol{\gamma}_y^2}}{\sqrt{\mathbf{f}_x^2 + \mathbf{f}_y^2}} \triangleq \frac{\boldsymbol{\gamma}_r}{\mathbf{f}_r} \tag{17}$$

However, equation (17) cannot be used directly to estimate d. Indeed, when the force control algorithm brings the force closed to zero, the estimation can become inaccurate due to the noise and resolution of the sensor. Therefore, we propose to use a weighted least-squares algorithm with a sliding window and a dead-zone to robustly estimate m and d (cf. [8]).

To minimize the estimation error, let's define the following cost function with sliding window and forgetting factor:

$$J(t, t_0) = \int_{\max(t-T, t_0)}^{t} e^{-\lambda(t-\tau)} \left[\boldsymbol{\gamma}_r(\tau) - \mathbf{f}_r(\tau)\widehat{m}(t)\right]^2 d\tau \tag{18}$$

where $\lambda > 0$ is a forgetting factor and $T > 0$ is the size of the sliding window. Then, the least-squares estimate $\widehat{m}(t)$ that minimizes $J(t, t_0)$ is equal to:

$$\widehat{m}(t) = R(t, t_0)^{-1} Q(t, t_0) \tag{19}$$

with:

$$R(t, t_0) = \int_{\max(t-T, t_0)}^{t} e^{-\lambda(t-\tau)} \mathbf{f}_r^2(\tau) d\tau \tag{20}$$

$$Q(t, t_0) = \int_{\max(t-T, t_0)}^{t} e^{-\lambda(t-\tau)} \mathbf{f}_r(\tau) \boldsymbol{\gamma}_r(\tau) d\tau \tag{21}$$

In practice, the estimate is not reliable when $\mathbf{f}_r$ or $\boldsymbol{\gamma}_r$ is closed to zero. Therefore, if $\mathbf{f}_r(t)$ or $\boldsymbol{\gamma}_r(t)$ decreases below some threshold value $\mathbf{f}_{th}$ or $\boldsymbol{\gamma}_{th}$, the computation of the least-squares estimate is frozen, *i.e.*, only the reference instrument velocity $\dot{d}^*$ along the $\mathbf{z}_t$ axis is taken into account. The least-squares estimate is computed only if the forces and torques are larger than the threshold values for a minimum length of time $T_0 \leq T$. Consequently, the robust estimation algorithm is defined as follows:

$$\widehat{d}(t) = \begin{cases} l - R(t, t_k)^{-1} Q(t, t_k) & \text{if } \mathbf{f}_r(t) > \mathbf{f}_{th},\ \boldsymbol{\gamma}_r(t) > \boldsymbol{\gamma}_{th} \\ & \text{and } t \geq t_k + T_0 \\ \widehat{d}(T_k) + \int_{T_k}^{t} \dot{d}^*(\tau) d\tau & \text{otherwise} \end{cases} \tag{22}$$

where t_k is the last time instant when $\mathbf{f}_r$ and $\boldsymbol{\gamma}_r$ left the dead-zone area, and T_k is the last time instant when $\mathbf{f}_r$ or $\boldsymbol{\gamma}_r$ entered the dead-zone area. Furthermore, since $0 < d < l$, a saturation function is applied on the estimate, so that it always stays in the interval $[0, l]$.

5.2 Experimental results

Figure 5 presents the experimental result for the direct estimation of d using the robust estimation algorithm. The experimental results are obtained with maximum size $T = 0.5$ sec of the sliding window and the minimum size $T_0 = 0.25$ sec. In order to compare these results with the previous ones, the experimental conditions for d_0 and d are reproduced. One can see that the convergence of the estimation algorithm is faster, as it does not involve any dynamics. The estimated signal d exhibits noise, that does not significantly affect the force response, as compared to Figure 4.

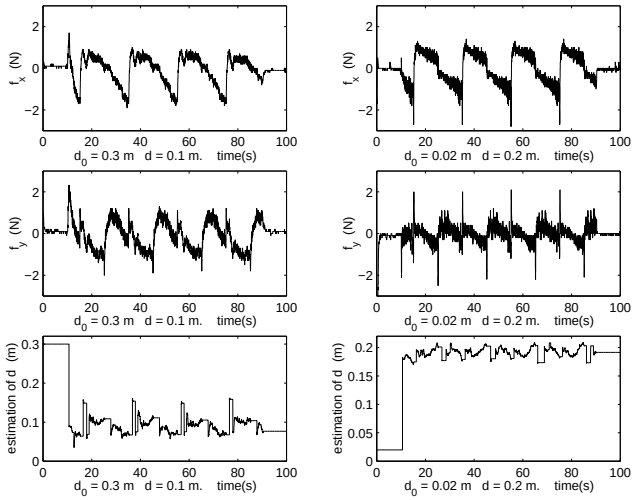

Figure 5: Experimental results with direct estimation of d

6 Conclusion

In this paper, we have proposed to use a 6 DOF actuated robot to hold surgical instruments for laparoscopic manipulation. Force feedback control strategies have been proposed to solve the trocar kinematic constraint, involving the on-line estimation of the environment geometry. They have been theoretically proven and experimentally validated. The functional improvement of such a method over existing systems has also been discussed in the introduction.

Acknowledgements

The financial support of the french ministry of research ("ACI Jeunes Chercheurs" program) is gratefully acknowledged.

References

[1] G. Guthart, J.K. Salisbury. The Intuitive TeleSurgery System: Overview and Applications *Proc*

of ICRA 2000, San Francisco, 2000.

[2] A. Madhani, G. Niemeyer and J.K. Salisbury. The Black Falcon: A Teleoperated Surgical Instrument for Minimally Invasive Surgery. *Proc. of the IEEE/RSJ Int. Conf. on Intelligent Robots and Systems (IROS)*, Victoria B.C., Canada, October, 1998.

[3] *http://www.computermotion.com*.

[4] A. Krupa, C. Doignon, J.Gangloff, M. de Mathelin, L. Soler and G. Morel. Towards semi-autonomy in laparoscopic surgery through vision and force feedback control. *Proc. of ISER'00: International Symposium on Experimental Robotics*, Hawaii, December, 2000.

[5] A. Krupa, M. de Mathelin, C. Doignon, J. Gangloff, G. Morel, L. Soler and J. Marescaux. Development of semi-autonomous control modes in laparoscopic surgery using visual servoing. *Proc. of MICCAI'01: International Conference on Medical Image Computing and Computer-Assisted Intervention*, Utretch, October, 2001.

[6] L. Villani, C. Canudas de Wit and B. Brogliato. An Exponentially Stable Adaptive Control for Force and Position Tracking of Robot Manipulators. *IEEE Transactions on Automatic Control*, vol 44, 4, pp 798-802, April 1999.

[7] L. Villani, C. Natale, B. Siciliano and C. Canudas de Wit. An Experimental Study of Adaptive Force/Position Control Algorithms for an Industrial Robot. *IEEE Transactions on Control Systems Technology*, vol 8, 5, pp 777-786, September 2000.

[8] M. de Mathelin and R. Lozano. Robust adaptive identification of slowly time-varying parameters with bounded disturbances. *Automatica*, vol. 35, pp. 1291-1305, July 1999.

[9] S. Sastry and M. Bodson. *Adaptive control: Stability, convergence, and robustness.* Prentice-Hall. Englewood Cliffs, NJ, 1989.

Appendix

Proof of Lemma 1 :

1. Let's define the following Lyapunov-like function:

$$V(t) = \frac{1}{2}e_p^2 = \frac{1}{2}(d-\widehat{d})^2 \geq 0 \tag{23}$$

Using (13) and (14), one gets:

$$\begin{aligned}\dot{V}(t) &= e_p\left(k_1(\dot{\mathbf{f}}_x + gk\mathbf{f}_x)\frac{\omega_y^*}{\epsilon+\omega_x^{*2}+\omega_y^{*2}}\right.\\ &\quad \left. - k_1(\dot{\mathbf{f}}_y + gk\mathbf{f}_y)\frac{\omega_x^*}{\epsilon+\omega_x^{*2}+\omega_y^{*2}}\right)\\ &= -k_1 g\left(\frac{\omega_x^{*2}+\omega_y^{*2}}{\epsilon+\omega_x^{*2}+\omega_y^{*2}}\right)e_p^2 \end{aligned}\tag{24}$$

Thus $\dot{V}(t) \leq 0$ and $V \in L_\infty$. Therefore, $\widehat{d}$ and $\dot{\widehat{d}} \in L_\infty$.

2. From equation (24), it follows that:

$$\int_0^\infty \frac{\omega_x^{*2}+\omega_y^{*2}}{\epsilon+\omega_x^{*2}+\omega_y^{*2}}e_p^2 dt = \frac{1}{k_1 g}(V(0)-V_\infty) \tag{25}$$

therefore, $\sqrt{\frac{\omega_x^{*2}+\omega_y^{*2}}{\epsilon+\omega_x^{*2}+\omega_y^{*2}}}e_p \in L_2$.

3. Since $V \geq 0$ and $\dot{V} \leq 0$, it follows that $V(t)$ is a monotically decreasing function bounded below by zero. Consequently, $\lim_{t\to\infty} V(t) = V_\infty$ and $\lim_{t\to\infty} e_p(t) = e_{p\infty}$.

4. From equation (24):

$$\dot{V}(t) = -2k_1 g\left(\frac{\omega_x^{*2}+\omega_y^{*2}}{\epsilon+\omega_x^{*2}+\omega_y^{*2}}\right)V(t) \tag{26}$$

Therefore, using Theorem 2.5.1 in [9], if $\sqrt{\frac{\omega_x^{*2}+\omega_y^{*2}}{\epsilon+\omega_x^{*2}+\omega_y^{*2}}}$ is persistently exciting, then $\lim_{t\to\infty} V(t) = 0$ exponentially, and $\lim_{t\to\infty} e_p = 0$ exponentially.

Proof of Lemma 2 :

1. Let's define the following Lyapunov-like function:

$$\begin{aligned}V(t) &= \frac{1}{2}\begin{bmatrix} d-\widehat{d} & g-\widehat{g}\end{bmatrix}\begin{bmatrix} g & 0\\ 0 & 1\end{bmatrix}\begin{bmatrix} d-\widehat{d}\\ g-\widehat{g}\end{bmatrix}\\ &= \frac{e_p^T A e_p}{2} \geq 0\end{aligned}\tag{27}$$

with $A = \begin{bmatrix} g & 0\\ 0 & 1\end{bmatrix}$. Using (13) and (16), one gets:

$$\dot{V}(t) = e_p^T A\dot{e}_p = -k_1 e_p^T \mathbf{Q} e_p \tag{28}$$

with:

$$\mathbf{Q} = \begin{pmatrix} g^2(\omega_x^{*2}+\omega_y^{*2}) & gk(\mathbf{f}_x\omega_y^* - \mathbf{f}_y\omega_x^*)\\ gk(\mathbf{f}_x\omega_y^* - \mathbf{f}_y\omega_x^*) & k^2\left(\mathbf{f}_x^2+\mathbf{f}_y^2\right)\end{pmatrix}$$

From the Sylvester's theorem, the quadratic function $\dot{V}(t)$ is semi-definite negative, if and only if, the upper left submatrices of $\mathbf{Q}$ have non-negative determinants. Since,

$$\begin{aligned}\mathbf{Q}_{11} &= g^2(\omega_x^{*2}+\omega_y^{*2}) \geq 0\\ det(\mathbf{Q}) &= g^2(k\mathbf{f}_x\omega_x^* + k\mathbf{f}_y\omega_y^*)^2 \geq 0\end{aligned}$$

therefore, $\mathbf{Q} \geq 0$, $\dot{V}(t) \leq 0$ and $V \in L_\infty$. It follows that $e_p \in L_\infty$ and, using equation (16), $\dot{\widehat{d}}$ and $\dot{\widehat{g}} \in L_\infty$.

2. From equations (13) and (16), we have:

$$\dot{e}_p = -k_1 \mathbf{Q} e_p \tag{29}$$

with $\mathbf{Q} = \mathbf{Q}^T \geq 0$, therefore if $\mathbf{Q}^{\frac{1}{2}}$ is persistently exciting, i.e.,

$$\exists \eta > 0 \;\; \exists T \;\; s.t. \;\; \frac{1}{T}\int_{t_0}^{t_0+T} \mathbf{Q} dt > \eta I > 0 \quad \forall t_0 \geq 0$$

using Theorem 2.5.1 in [9], then $\lim_{t\to\infty} \dot{e}_p = 0$, exponentially.